ISSN 0031-0301, Paleontological Journal, 2024, Vol. 58, No. 7, pp. 752–766. © Pleiades Publishing, Ltd., 2024.

Micropaleontological Markers for the Stratigraphy of Upper Pleistocene–Holocene Deposits in the Southeastern Part of the Sea of Okhotsk (Based on Radiolarian Analysis)

L. N. Vasilenko[a], *, Yu. P. Vasilenko[a], **, and S. A. Gorbarenko[a], ***

[a] *Il'ichev Pacific Oceanological Institute, Far East Branch, Russian Academy of Sciences, Vladivostok, 690043 Russia*

**e-mail: lidia@poi.dvo.ru*

***e-mail: vasilenko@poi.dvo.ru*

****e-mail: gorbarenko@poi.dvo.ru*

Received February 12, 2024; revised February 26, 2024; accepted February 26, 2024

Abstract—The distribution of radiolarians in core LV76-9-1 (southeastern part of the Sea of Okhotsk) is studied. Based on a developed age model of the core, we established the biostratigraphic levels of some key radiolarian species and correlated them with the central part of the Sea of Okhotsk. Changes in the qualitative and quantitative characteristics of radiolarians are recorded during marine isotope stages 5–1. The species *Lychnocanoma sakaii* Morley et Nigrini, 1995, *Cycladophora davisiana* Ehrenberg, 1861, and *Cerathospyris borealis* Bailey, 1856, which are predominant in the Sea of Okhotsk, are divided into morphological forms, and the concentrations of these forms in deposits over the past 122 kyr are established.

Keywords: radiolarians, biostratigraphy, Sea of Okhotsk, dated levels, marine isotopic stages

DOI: 10.1134/S0031030124600422

INTRODUCTION

It is impossible to perform paleoceanological reconstructions without a time reference (age models of sediment cores, stratigraphic schemes and scales, etc.) for the phenomena and events under study. The current state of science requires increasingly detailed references with ever-greater time resolution. This especially applies to the development of age models of cores of Upper Pleistocene–Holocene deposits, which serve as a basis for studying centennial (up to multidecadal) changes in the marine environment and climate. Common tools used to develop age models for deposits of this age are radioisotope methods and oxygen-isotope and paleomagnetic scales. Modern technologies have made it possible to extend the range of application of the radiocarbon method from 24 ka to almost 50 ka. However, the increase in the age of the studied carbonate material also involves an increase in the error of the method. This is due to the authigenic transformation of carbonate material, the introduction of "old" organic matter, inaccuracies in determining the reservoir effect, etc. In addition, radiocarbon dating is inapplicable to sediments collected below the carbonate compensation level; therefore, older deposits cannot be dated by this method. This requires the use of additional methods, in particular, for Upper Pleistocene deposits. Other radioisotope methods also have certain drawbacks. The existing paleomagnetic scales most often require serious modification for high-resolution reconstructions. Thus, the difference between the same paleomagnetic excursions according to different scales can be several thousands of years (e.g., Yamamoto et al., 2007; Channell et al., 2009). Another factor that does not allow the construction of high-resolution age models based on paleomagnetic scales is the extremely small number of paleomagnetic excursions in the Upper Pleistocene–Holocene deposits. Therefore, paleomagnetic scales for age models of such deposits can only be used to establish a small set of key points, and even then, with great caution. At the present time, the most effective tool is the correlation with oxygen-isotope scales constructed based on the study of ice cores (North Greenland..., 2004; Wolff et al., 2010; etc.) or cave stalagmites (Chen et al., 2016, 2022). However, the construction of age models based on this principle requires very considerable experience from the scientist, as well as good knowledge of the paleoenvironmental conditions of the study region. An invaluable aid to the development of age models based on such correlations, which greatly simplify this work, is the use of additional control age points which can be obtained by other chronostratigraphic methods.

Radiolarian analysis is one of the key methods for reconstructing the environmental conditions of seas and oceans. Since radiolarians have rapid speciation

and their siliceous skeletons are well preserved in sediments, they are actively used for biostratigraphy and paleoceanology, in particular, for studying the Sea of Okhotsk (Ling, 1974; Kruglikova, 1975; Tsoy and Shastina, 2000, 2005; Matul, 2002, 2009; Okazaki et al., 2003, 2004, 2006; Itaki et al., 2008; Yanchenko and Gorbarenko, 2015; Yanchenko, 2019; etc.). The levels of first occurrence (FO), last occurrence (LO), and last common occurrence (LCO) of key radiolarian species are of fundamental importance not only for determining the age of deposits, but also for identifying regional and global changes in the natural environment (climate, hydrological, and tectonic changes). In the Sea of Okhotsk, these dated levels are consistent with Pleistocene paleoclimatic events (Matul, 2009).

The complicate circulation system and other factors led to different levels of productivity of radiolarians in the western and eastern parts of the Sea of Okhotsk, both in the past and in the present (*Gidrometeorologiya*..., 1996; *Kompleksnye issledovaniya*..., 1997; Shuntov, 2001; Bosin et al., 2015; etc.). This was reflected in differences between the dated levels of radiolarian species depending on the study area (Kruglikova, 1975; Takahashi et al., 2000; Matul et al., 2002, 2009; Okazaki et al., 2003). Therefore, it is important to spatially study the Sea of Okhotsk to obtain the general picture of how these levels are manifested in remote areas and what processes might influence their differences.

The purpose of our study is to identify biostratigraphic markers for constructing and detailing the age models of the eastern part of the Sea of Okhotsk and adjacent areas.

MATERIAL AND METHODS

The material for the study was sediment core LV76-9-1, which was obtained during the Russian–Chinese expedition on the R/V Akademik M.A. Lavrentiev in 2016 (location: 50°29.21′ N, 153°24.05′ E, sea depth 924 m, core depth 870 cm) (Fig. 1). Every fourth centimeter was studied; a total of 218 samples (436 preparations) were studied.

Preparation samples and establishment of the quantitative characteristics of radiolarians were based on the method by Abelmann (1988), Abelmann et al. (1999).

The total radiolarian content (TRC), taxonomic composition, species richness (number of radiolarian taxa in a sample), and relative abundance of each taxon (%) were determined in the preparations using a LOMO Mikmed-6 microscope.

Collection no. 76 of radiolarians of the Upper Pleistocene–Holocene is deposited at the Laboratory of Marine micropaleontology of the Il'ichev Pacific Oceanological Institute, Far East Branch, Russian Academy of Sciences.

AGE MODEL

The preliminary age model of core LV76-9-1 was constructed based on a multi-proxy approach. The age model was developed using the results of analyzes of $\delta^{18}O$ and $\delta^{13}C$ in the shells of planktonic and benthic foraminifers, paleomagnetic parameters (ChRM/ARM and Ch_Jrs), and variations in magnetic susceptibility, as well as data of analyzes of paleoproductivity indicators (contents of chlorine, total organic carbon (TOC), and $CaCO_3$).

To establish the boundaries between marine isotope stages (MIS), we used a graphical correlation between the relative sea level (RSL) stack (Spratt and Lisiecki, 2016) and the $\delta^{18}O$ record from benthic foraminifer shells from core LV76-9-1 averaged over five values (Figs. 2*A* (blue line), 2*H*). The RSL stack summarizes several $\delta^{18}O$ records from the shells of carbonate microorganism, predominantly benthic foraminifers, from sediment cores collected in different regions of the World Ocean. This correlation makes it possible to fairly reliably establish the boundaries between MISs (Fig. 2). We accepted the ages for the boundaries between MISs according to Martinson et al. (1987) and Wolff et al. (2010): 28 ka between MIS 2 and MIS 3, 59 ka between MIS 3 and MIS 4, 73.9 ka between MIS 4 and MIS 5, 85 ka between MIS 5.1 and MIS 5.2, 93 ka between MIS 5.2 and MIS 5.3, 105 ka between MIS 5.3 and MIS 5.4, and 117 ka between MIS 5.4 and MIS 5.5 (Table 1, Fig. 2). We included the beginning of deglaciation in MIS 1. Accordingly, we established the boundary between MIS 1 and MIS 2 as 14.7 ka (Table 1, Fig. 2).

In addition to the graphical correlation with the RSL stack, we also used the well-known patterns of change in indicators of productivity and magnetic susceptibility in the Sea of Okhotsk during the identification of the boundaries between MISs (Gorbarenko, 1996; Gorbarenko et al., 2002a, 2002b, 2007, 2012; Vasilenko et al., 2017). Thus, the boundary between MIS 1 and MIS 2 that we accepted is clearly marked by a sharp increase in the values of productivity indicators and a decrease in the values of magnetic susceptibility (Gorbarenko, 1996; Gorbarenko et al., 2002a, 2002b) (Figs. 2*C*, 2*D*, 2*E*). The boundary between MIS 2 and MIS 3 is characterized by a decrease in the values of TOC and chlorine content and a simultaneous increase in the level of magnetic susceptibility (Gorbarenko, 1996; Gorbarenko et al., 2002b, 2007, 2012) (Figs. 2*C*, 2*D*, 2*E*). The magnetic susceptibility of bottom sediments in the eastern part of the Sea of Okhotsk, accumulated in MIS 3, has a specific pattern characterized by a series of sharp peaks. These peaks are determined by relatively short-term episodes of supply of terrigenous material to this area of the sea (Sakamoto et al., 2005; Nürnberg et al., 2011; Vasilenko et al., 2017). This feature makes it possible to more accurately determine the boundaries for MIS 3 (Fig. 2*F*). In addition, according to paleomagnetic

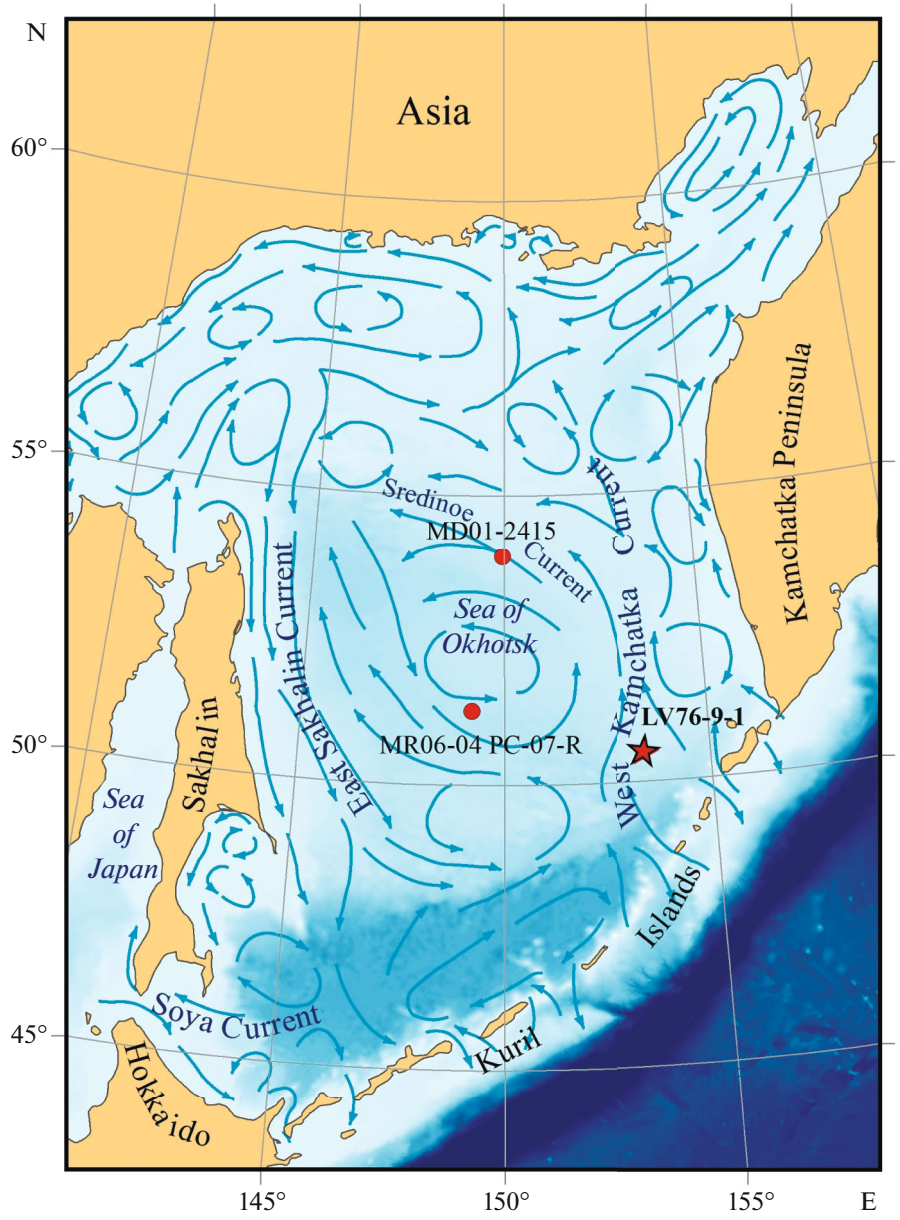

Fig. 1. Location of Cores LV76-9-1 (this study, marked with an asterisk), MD01-2415 (Matul et al., 2009, marked with a circle), and MR06-04PC-07-R (Yanchenko and Gorbarenko, 2015, Yanchenko, 2019, marked with a circle). The scheme of surface currents is given according to Chernyavskii (*Kompleksnye issledovaniya*..., 1997). The topographical basis was taken from the GEBCO website (https://www.gebco.net).

analysis, core LV 76-9-1 shows the Laschamp paleomagnetic excursion at a horizon of 260 cm, the age of which is estimated at 41 ka (Channel et al., 2018) (Fig. 2*G* (gray vertical line)). The boundaries between MIS 5.1 and MIS 5.4 are confirmed by the values of magnetic susceptibility: warm MIS 5.1 and MIS 5.3 have lower values than cold MIS 5.2 and MIS 5.4 (Fig. 2*F*). In addition, the boundaries between

Fig. 2. Correlation of changes in $\delta^{18}O$ (blue curve shows averaging over the five values) (A) and $\delta^{13}C$ (B), concentrations of $CaCO_3$ (C), TOC (D), and Chlorin (E), and variations in magnetic susceptibility (F) and ChRM/ARM (blue curve) and Ch_Jrs (red curve) of core LV76-9-1 (G) with relative sea level stack (H) (Spratt and Lisiecki, 2016) and with $\delta^{18}O$ records from core NGRIP (I) (Wolff et al., 2010). Solid lines indicate the boundaries of marine oxygen-isotope stages (MISs); dotted lines with large intervals indicate the boundaries between the substages of MIS 5; dotted lines with small intervals indicate the position of interstadials (ISs); gray line shows the position of the Laschamp paleomagnetic intensity excursion.

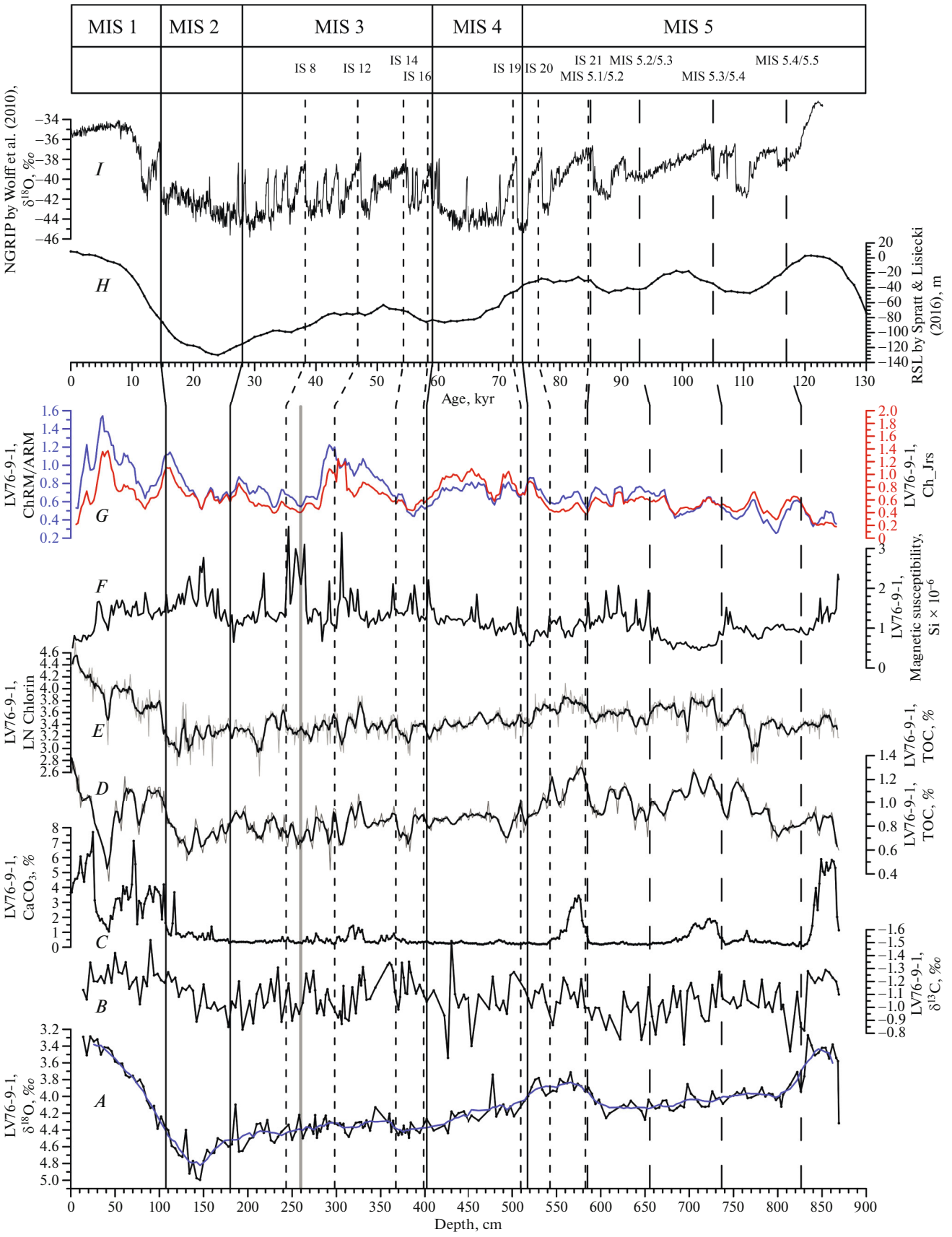
MIS 1
MIS 2
MIS 3
MIS 4
MIS 5
IS 8
IS 12
IS 14
IS 16
IS 19
IS 20
IS 21
MIS 5.2/5.3
MIS 5.1/5.2
MIS 5.3/5.4
MIS 5.4/5.5
NGRIP by Wolff et al. (2010), δ18O, ‰
I
H
RSL by Spratt & Lisiecki (2016), m
Age, kyr
LV76-9-1, ChRM/ARM
G
LV76-9-1, Ch_Jrs
F
LV76-9-1, Magnetic susceptibility, Si × 10−6
LV76-9-1, LN Chlorin
E
LV76-9-1, TOC, %
D
LV76-9-1, TOC, %
LV76-9-1, CaCO3, %
C
B
LV76-9-1, δ13C, ‰
LV76-9-1, δ18O, ‰
A
Depth, cm

Table 1. Key points for constructing the age model along core LV76-9-1

Events	Age of key points, ka	Depth, cm
Ash KO	8.46	38
	8.47	44
Beginning of Bølling–Allerød/Boundary between MIS 1 and MIS 2	14.69	107
Boundary between MIS 3 and MIS 2	28	180
Interstadial 8	38.22	243
Laschamp	41	260
Interstadial 12	46.86	298
Interstadial 14	54.22	367
Interstadial 16	58.28	399
Boundary between MIS 4 and MIS 3	59	403
Interstadial 19	72.33	509
Boundary between MIS 5 and MIS 4	73.9	518
Interstadial 20	77.8	543
Interstadial 21	84.7	584
Boundary between MIS 5.1 and MIS 5.2	85	586
Boundary between MIS 5.2 and MIS 5.3	93	656
Boundary between MIS 5.3 and MIS 5.4	105	737
Boundary between MIS 5.4 and MIS 5.5	117	827

MIS 5.1 and MIS 5.2 and between MIS 5.3 and MIS 5.4 are confirmed by a sharp increase in $CaCO_3$ content (Fig. 2*C*).

Previously, the study of long-term interstadials (IS) of the Dansgaard–Oeschger cycles revealed a sharp and relatively significant increase in productivity in the northern part of the Pacific Ocean and its marginal seas during such ISs (Tada et al., 1999; Hendy and Kennett, 2003; Gorbarenko et al., 2004, 2005, 2007; Harada et al., 2006; Riethdorf et al., 2013). Based on this pattern, we compared the records of paleoproductivity indicators and $\delta^{18}O$ record from core LV76-9-1 with the $\delta^{18}O$ record from the Greenland ice core (North Greenland..., 2004; Wolff et al., 2010) to identify the position of sediment horizons accumulated during long-term ISs. As a result, we established the

Explanation of Plate 1

Sea of Okhotsk: Upper Pleistocene–Holocene, core LV76-9-1. Representatives of Collodaria (figs. 1–3) and Spumellaria (figs. 4–18). Scale bar: 100 μm.

Fig. 1. *Acrosphaera* ex gr. *arktios* (Nigrini, 1970), F.1, specimen POI, no. 76-860/2-4, core depth of 860–861 cm.

Fig. 2. *Acrosphaera* ex gr. *arktios* (Nigrini, 1970), F.2, specimen POI, no. 76-48/2-2, core depth of 48–49 cm.

Fig. 3. *Acrosphaera* ex gr. *pseudoarctios* Caulet, 1986, specimen POI, no. 76-856/2-1, core depth of 856–57 cm.

Fig. 4. *Stylosphaera lithatractus* Haeckel, 1887, specimen POI, no. 76-836/1-1, core depth of 836–37 cm.

Fig. 5. *Druppatractus* sp., specimen POI, no. 76-856/1-5, core depth of 856–857 cm: (5a) focus on the pores, (5b) focus on the inner part of the skeleton.

Fig. 6. *Stylatractus* cf. *neptunus* Haeckel, 1887, specimen POI, no. 76-644/2-1, core depth of 644–645 cm.

Fig. 7. *Echinomma popofskii* Petrushevskaya, 1967, specimen POI, no. 76-200/1-2, core depth of 200–201 cm.

Fig. 8. *Rhizoplegma boreale* (Cleve, 1899), specimen POI, no. 76-320/1-1, core depth of 320–321 cm.

Fig. 9. *Actinomma boreale* Cleve, 1899, specimen POI, no. 76-320/1-4, core depth of 320–321 cm.

Fig. 10. *Cenosphaera cristata* Haeckel, 1887, specimen POI, no. 76-856/1-3, core depth of 856–857 cm.

Fig. 11. *Cromyechinus borealis* (Cleve, 1898), specimen POI, no. 76-180/1-2, core depth of 180–181 cm.

Fig. 12. *Larcopyle bütschlii* Dreyer, 1889, specimen POI, no. 76-860/2-12, core depth of 860–861 cm.

Figs. 13, 14. Pyloniidae spp.: (13) specimen POI, no. 76-420/1-1, core depth of 420–421 cm, (14) specimen POI, no. 76-48/1-2, depth of 48–49 cm.

Fig. 15. *Lithelius minor* Jørgensen, 1900, specimen POI, no. 76-216/2-3, core depth of 216–217 cm.

Fig. 16. *Spongotrochus glacialis* Popofsky, 1908, specimen POI, no. 76-268/2-1, core depth of 268–269 cm.

Fig. 17. *Stylochlamidium venustum* (Bailey, 1856), specimen POI, no. 76-36-5, core depth of 36–37 cm.

Fig. 18. *Spongopyle osculosa* Dreyer, 1889, specimen POI, no. 76-864/1-7, core depth of 864–865 cm.

Plate 1

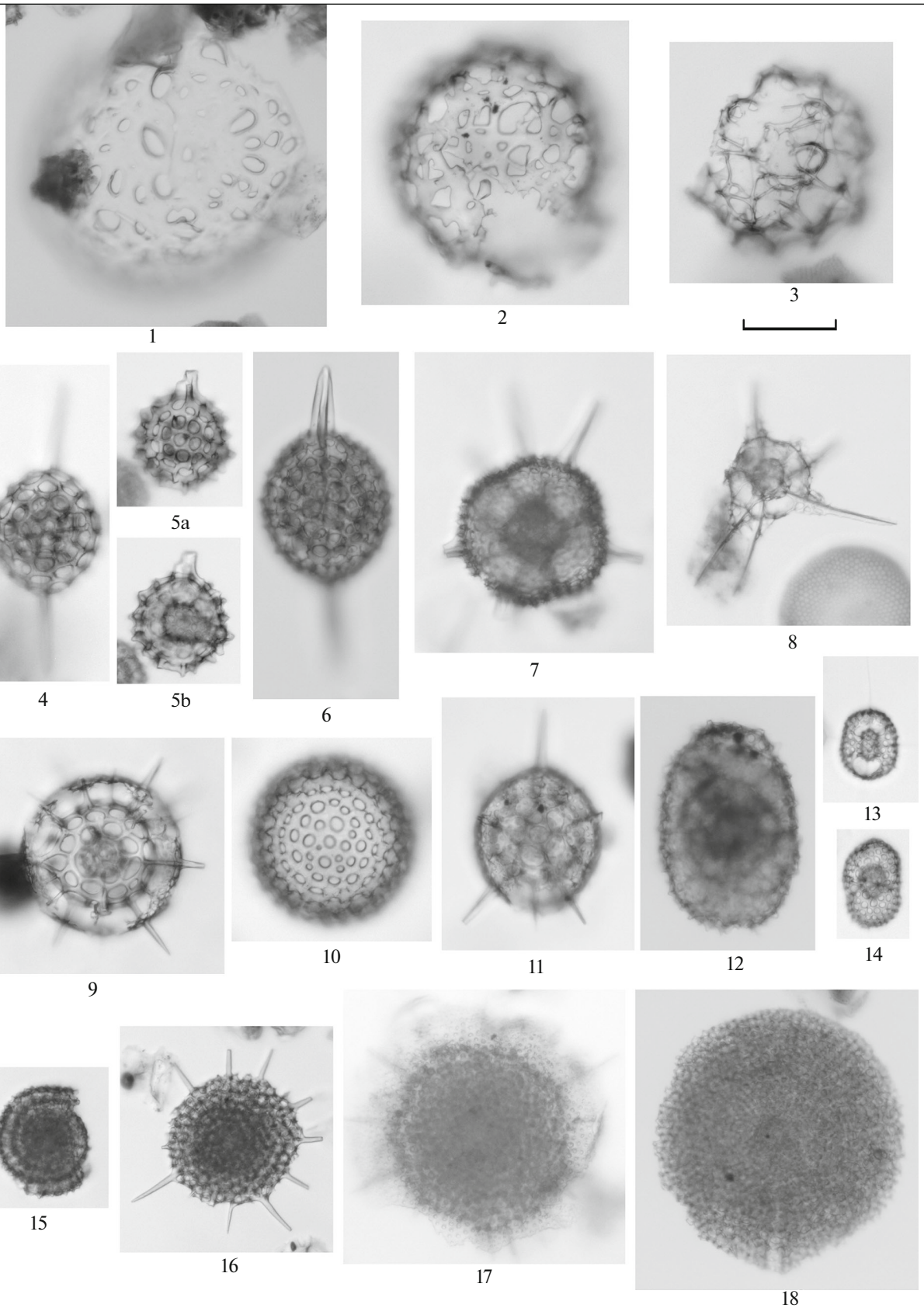

position of IS 8, IS 12, IS 14, IS 16, and IS 19–IS 21 within the corresponding MISs for sediments from core LV76-9-1 (Table 1; Figs. 2*A*, 2*C*, 2*D*, 2*E*, 2*I*).

GENERAL CHARACTERISTICS OF THE TAXONOMIC COMPOSITION OF RADIOLARIANS IN CORE LV76-9-1

We recorded 129 species and infrageneric taxa of radiolarians in the sediments of core LV76-9-1 (5 Collodaria taxa, 50 Spumellaria taxa, and 74 Nassellaria taxa). Almost all the species that we identified were established in the Sea of Okhotsk earlier with some variations in their abundance (Kruglikova, 1975, 2013; Nimmergut and Abelmann, 2002; Okazaki et al., 2003; Itaki et al., 2008; Matul, 2009; Yanchenko and Gorbarenko, 2015, Yanchenko, 2019, etc.). Previously, S.B. Kruglikova (1975) noted that radiolarians from the Sea of Okhotsk had a significant morphological variability. We also drew attention to the existing differences in some specimens belonging to the same species according to the morphological features (Vasilenko et al., 2023). Generally, these are species with a high abundance in the assemblage: *Cycladophora davisiana* Ehrenberg, 1861 (up to 50%), *Lychnocanoma sakaii* Morley et Nigrini, 1995 (up to 70%), and *Cerathospyris borealis* Bailey, 1856 (up to 18.4%). Differences are also observed for specimens of the species *Acrosphaera arktios* (Nigrini, 1970), the proportion of which is low in the assemblage (0.1–0.6%). The morphological features of the above species allowed us to divide each of them into two morphoforms: *A. arktios* F.1 and *A. arktios* F.2 differ in porosity (Pl. 1, figs. 1, 2); *C. davisiana* F.1 and *C. davisiana* F.2 differ in the shape of the thorax and a smaller size of the pores on the thorax in the latter (Pl. 2, figs. 18, 19); *L. sakaii* F.1 and *L. sakaii* F.2 differ in the presence of a fourth lateral spine in the latter (Pl. 2, figs. 1, 2); and *C. borealis*

Explanation of Plate 2

Sea of Okhotsk: Upper Pleistocene–Holocene, core LV76-9-1. Representatives of Nassellaria. Scale bar: 100 μm.

Fig. 1. *Lychnocanoma sakaii* Morley et Nigrini, 1995, F.1, specimen POI, no. 76-860/2-5, core depth of 860–861 cm.

Fig. 2. *Lychnocanoma sakaii* Morley et Nigrini, 1995, F.2, specimen POI, no. 76-684/2-9, core depth of 684–685 cm.

Fig. 3. *Dictyophimus* sp., specimen POI, no. 76-336/2-2, core depth of 336–337 cm.

Fig. 4. *Pterocanium corotnevi* (Dogiel et Reshetnyak, 1952), specimen POI, no. 76-684/2-7, core depth of 684–685 cm.

Fig. 5. *Cyrtopera laguncula* Haeckel, 1887, specimen POI, no. 76-124/1-1, core depth of 124–125 cm.

Fig. 6. *Callimitra* (?) sp., specimen POI, no. 76-660/2-4, core depth of 660–661 cm.

Fig. 7. *Dictyophimus macropterus* (Ehrenberg, 1873), specimen POI, no. 76-164/1-2, core depth of 164–165 cm.

Fig. 8. *Sethoconus tabulatus* (Ehrenberg, 1873), specimen POI, no. 76-852/2-7, core depth of 852–853 cm.

Fig. 9. *Artobotrys borealis* (Cleve, 1899), specimen POI, no. 76-864/1-1, core depth of 864–865 cm.

Fig. 10. *Amphimelissa setosa* (Cleve, 1899), specimen POI, no. 76-860/2-1, core depth of 860–861 cm.

Fig. 11. *Botryocampe inflata* (Bailey, 1956), specimen POI, no. 76-540/2-1, core depth of 540–541 cm.

Fig. 12. *Botryocampe robusta* (Kruglikova, 1975), specimen POI, no. 76-560/2-2, core depth of 560–61 cm.

Fig. 13. *Pterocorys* sp., specimen POI, no. 76-336/2-1, core depth of 336–337 cm.

Fig. 14. *Lophophaena witjazii* (Petrushevskaya, 1971) Van de Paverd, 1995, specimen POI, no. 76-852/2-6, core depth of 852–853 cm.

Fig. 15. *Pseudocubus* sp. F.1, specimen POI, no. 76-340/2-1, core depth of 340–341 cm.

Fig. 16. *Trisulcus* sp. F.1, specimen POI, no. 76-852/1-1, core depth of 852–853 cm.

Fig. 17. *Trisulcus* sp. F.2, specimen POI, no. 76-288/1-2, core depth of 288–289 cm.

Fig. 18. *Cycladophora davisiana* Ehrenberg, 1861, F.1, specimen POI, no. 76-860/1-5, core depth of 860–861 cm.

Fig. 19. *Cycladophora davisiana* Ehrenberg, 1861, F.2, specimen POI, no. 76-664/1-1, core depth of 664–665 cm.

Fig. 20. *Cycladophora* cf. *robusta* Lombari et Lazarus, 1988, specimen POI, no. 76-684/2-6, core depth of 684–685 cm.

Figs. 21, 22. *Cycladophora* sp.: (21) specimen POI, no. 76-36-3, depth of 36–37 cm, (22) specimen POI, no. 76-184/2-2, core depth of 184-185 cm.

Fig. 23. *Cycladophora cornuta* (Bailey, 1856), specimen POI, no. 76-340/2-4, core depth of 340–341 cm.

Fig. 24. *Clathrocycloma* sp., specimen POI, no. 76-320/1-3, core depth of 320–321 cm.

Fig. 25. *Lithocampe platycephala* (Ehrenberg, 1873), specimen POI, no. 76-688/1-1, core depth of 688–689 cm.

Fig. 26. *Botryostrobus aquilonaris* (Bailey, 1856), specimen POI, no. 76-864/2-16, core depth of 864–865 cm.

Fig. 27. *Artostrobium botryocyrtium* (Haeckel, 1887), specimen POI, no. 76-356/1-1, core depth of 356–357 cm.

Fig. 28. *Siphocampe arachnea* (Ehrenberg, 1862), specimen POI, no. 76-868-6, core depth of 868–869 cm.

Fig. 29. *Lithomitra lineata* Ehrenberg, 1839, specimen POI, no. 76-20-4, core depth of 20–21 cm.

Fig. 30. *Dumetum rectum* Popofsky, 1908, specimen POI, no. 76-336/1-1, core depth of 336–337 cm.: (30a) focus on the anterior part of the skeleton, (30b) focus on the posterior part of the skeleton.

Fig. 31. *Cerathospyris borealis* Bailey, 1856, F.1, specimen POI, no. 76-36/1-3, core depth of 36–37 cm.

Fig. 32. *Cerathospyris borealis* Bailey, 1856, F.2, specimen POI, no. 76-864/2-11, core depth of 864–865 cm.: (32a) focus on the pores, (32b) focus on the skeleton contour.

Fig. 33. *Cerathospyris spinosus* (Kruglikova, 1974), specimen POI, no. 76-860/1-4, core depth of 860–861 cm.

Plate 2

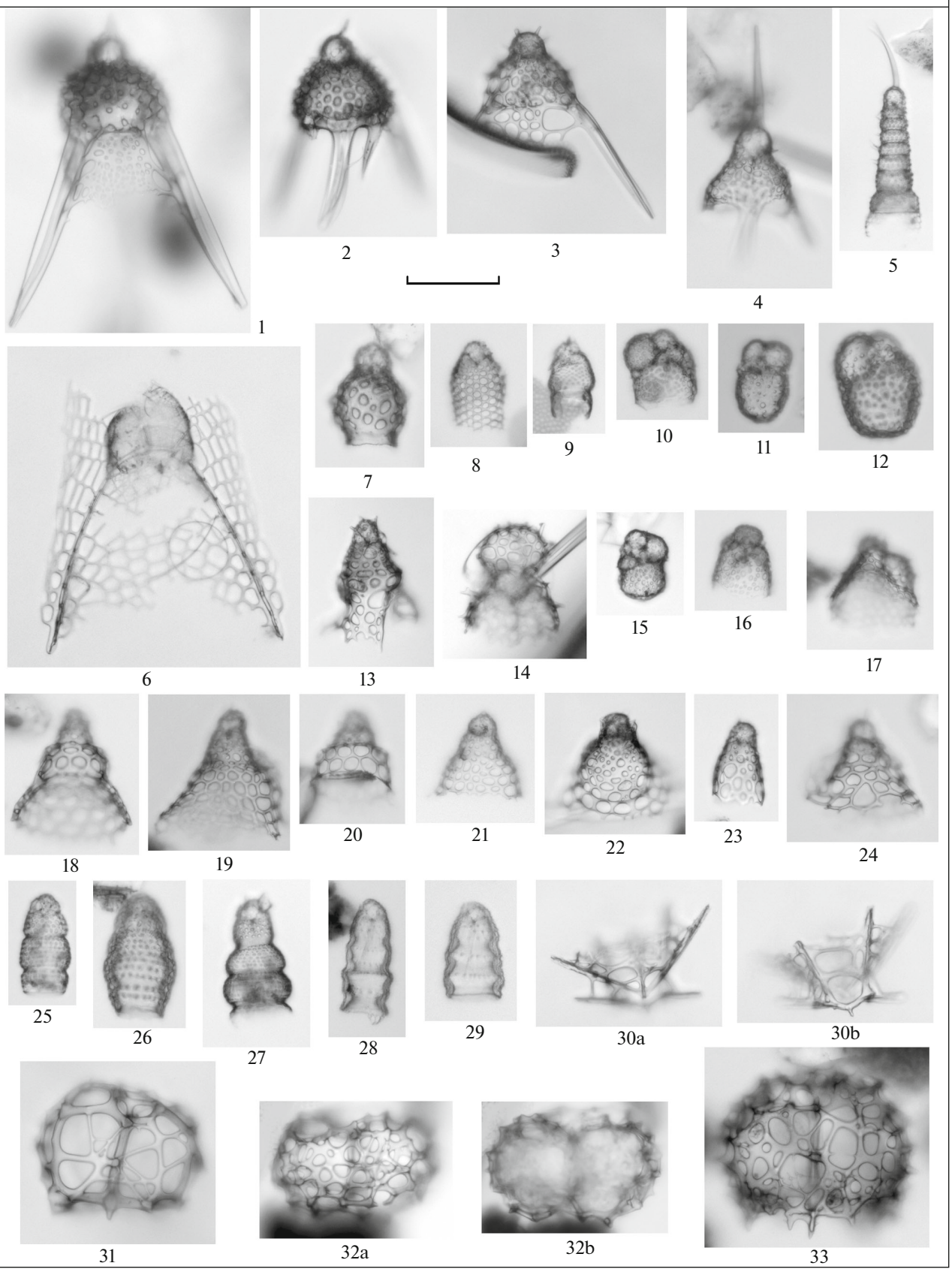
1
2
3
4
5
6
7
8
9
10
11
12
13
14
15
16
17
18
19
20
21
22
23
24
25
26
27
28
29
30a
30b
31
32a
32b
33

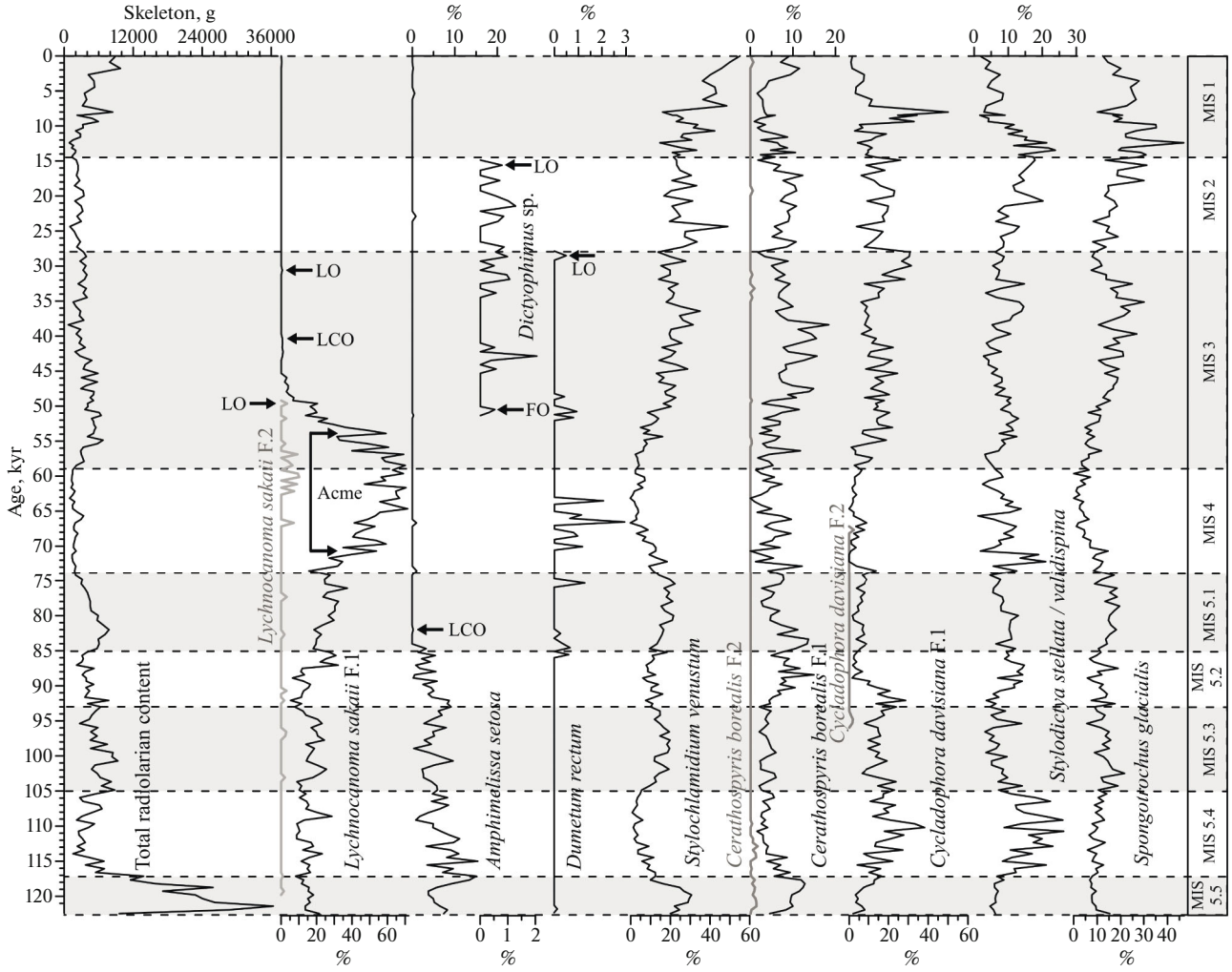

Fig. 3. Total content of radiolarians and distribution of some species in core LV76-9-1. FO—first occurrence, LO—last occurrence, LCO—last common occurrence, Acme—maximum content level.

F.1 and *C. borealis* F.2 differ in the horizontally elongated (dumbbell-like) shape of the latter and its smaller and more frequent pores (Pl. 2, figs. 31, 32a, 32b). In addition to the above species, the following species are also recorded in high abundance: *Stylochlamidium venustum* (Bailey, 1856) (up to 55.2%), *Spongotrochus glacialis* Popofsky, 1908 (up to 46.8%), the *Stylodictya stellata* Bailey, 1856/*validispina* Jørgensen, 1905 species group (up to 26.3%), *Amphimelissa setosa* (Cleve, 1899) (up to 15.4%), *Siphocampe arachnea* (Ehrenberg, 1862) (up to 9.8%), and *Larcopyle bütschlii* Dreyer, 1889 (up to 8.8%).

VARIATIONS OF RADIOLARIAN ASSEMBLAGES ON AN ORBITAL SCALE

The content of radiolarians in core LV76-9-1 reflects the generally accepted trend towards a decrease in total abundance during glacial periods and its increase during interglacial periods (Fig. 3).

In the warm MIS 5.5 interval (869–828 cm, about 122–117 kyr), the radiolarian assemblage is characterized by the highest TRC values, which range from 9574 to 36380 skeletons/g, and taxonomic composition, which includes 85 taxa. This interval is dominated by the species *S. venustum* (9.9–30.7%) and *L. sakaii* F.1 (8.2–21.6%). High levels of abundance are also recorded for the taxa *C. davisiana* F.1 (2.0–16.6%), *S. glacialis* (6.8–15.3%), *C. borealis* F.1 (5.6–12.8%), and *A. setosa* (3.8–15.1%), the *S. stellata/validispina* group (4.7–8.8%), *Tholospyra* sp. F.1 (2.6–5.7%), *Cerathospyris spinosus* (Kruglikova, 1974) (0.8–4.6%), and *Tholospyra* sp. F.2 (0.3–4.1%). In addition, the following species are constantly recorded at low abundance: *L. bütschlii* (0.2–1.8%), *Spirema haliomma* (Ehrenberg, 1862) (0.2–1.8%), *Lithelius minor* Jørgensen, 1905 (0.3–0.9%), *Spongurus pylomaticus* Riedel, 1958 (0.4–2.3%), *Botryostrobus aquilonaris* (Bailey, 1856) (0.4–2.2%), *S. arachnea* (0.2–2.1%), *Lithomitra lineata* Ehrenberg, 1839 (0.3–1.2%), etc. A

single occurrence of the taxa *A. arktios* F.1, *Acrosphaera pseudoarctios* Caulet, 1986, *Collosphaera* sp., *Spongodiscus biconcavus* Haeckel, 1887, *Cycladophora urymensis* (?) Popova, 1989, and *Cycladophora bicornis klingi* Lombari et Lazarus, 1988 is recorded in this interval; they are absent higher up along the core length.

In the cold MIS 5.4 interval (825–740 cm, about 117–105 kyr), the TRC sharply decreases to 1539–6927 skeletons/g; the taxonomic composition includes 70 taxa. The abundance of the species *S. venustum* significantly decreases (0.8–12.4%) and that of *L. sakaii* F.1 slightly increases (8.8–28.7%) in this interval. The species *C. davisiana* F.1 becomes dominant in the assemblage (4.0–38.2%). The abundance of the *S. stellata/validispina* species group also sharply increases (8.4–26.3%). The abundance of the species *A. setosa* significantly varies from 0.9 to 15.4% and forms frequent peaks. The taxa *Cromyechinus antarctica* (Dreyer, 1889), *Cornutella profunda* Ehrenberg, 1856, *Artostrobus jørgensenii* Petrushevskaya, 1967, *Clathromitrinae* sp., *Lipmanella dictyoceras* (Haeckel, 1861), and *Pterocanium* sp. F.1 occur for the last time in this interval.

In the warm MIS 5.3 interval (737–656 cm, about 105–93 kyr), TRC slightly increases to 2684–9330 skeletons/g; however, the taxonomic diversity continues to decrease and includes 68 taxa. The assemblage is dominated by *L. sakaii* F.1 (7.7–25.6%). The abundance of the species *S. glacialis*, *L. bütschlii*, *S. venustum*, and *S. arachnea* increases (5.6–21.6%, 1.7–7.0%, 5.5–19.8%, and 0.4–6.9%, respectively), while the assemblage of the taxon *C. davisiana* F.1 (6.5–24.0%), *S. stellata/validispina* species group, and taxa *C. borealis* F.1 and *A. setosa* decreases again (3.3–14.2%, 2.0–6.0%, and 0.4–9.7%, respectively). The species *Druppatractus ostracion* Haeckel, 1887, *S. haliomma*, *Artobotrys borealis* (Cleve, 1899), and *Trisulcus* sp. F.1 are recorded for the last time in this interval.

In the cold MIS 5.2 interval (653–588 cm, about 93–85 kyr), the TRC and their taxonomic composition continue to decrease (2159–7734 skeletons/g and 53 taxa). The abundance of *L. sakaii* F.1 slightly decreases (to 5.3–16.5%) in this interval and sharply increases to 22.1–32.2% by the end of MIS 5.2. In addition, the abundance of the species *A. setosa* gradually decreases, which is 1.4% by the end of MIS 5.2 (Fig. 3). The species *C. borealis* F.1 and *C. davisiana* F.1 form sharp peaks of abundance (the former in the middle of the interval and the latter at the beginning of the interval), followed by their sharp decrease. This interval contains the species *Actinomma leptodermum longispinum* (Cortese et Bjørklund, 1998), which was not found in either the underlying or the overlying intervals.

At the beginning of the warm MIS 5.1 period (585–520 cm, about 85–73.9 kyr), TRC increases to 7790 skeletons/g, followed by its gradual decrease to 1971 skeletons/g at the MIS 5.1–MIS 4 boundary. The taxonomic composition includes 55 taxa. The assemblage is dominated by *L. sakaii* F.1 (18.1–37.4%). The level of last common occurrence (LCO) of *A. setosa* is recorded in this interval. No sharp change is recorded in the abundance of other species: *C. davisiana* F.1 (1.6–9.0%), *C. borealis* F.1 (2.5–13.6%), *S. stellata/validispina* (5.6–13.0%), and *S. venustum* (9.5–22.3%). The species *Dipylissa bensoni* Dumitrica, 1988, *Gondvanaria* sp., and *Mitrocalpis araneafera* Popofsky, 1908 occur for the last time in this interval. The assemblage also contains the species *Lophophaena nadezdae* Petrushevskaya, 1971, which was not found in either the underlying or overlying intervals.

In the cold MIS 4 interval (517–404 cm, about 73.9–59 kyr), we observe the lowest TRC values (957–3360 skeletons/g); the taxonomic composition includes 54 taxa. The abundance of *L. sakaii* F.1 sharply increases to 71.2%. In addition, multiple individual peaks of the abundance of *Dumetum rectum* Popofsky, 1908 (0.6–2.9%) are recorded (Fig. 3). The taxa *C. davisiana* F.2 and *Pseudodictyophimus* sp. occur for the last time in this interval.

In the warm MIS 3 interval (401–180 cm, about 59–28 kyr), TRC increases to 6739 skeletons/g in the first half and decreases by almost 2 times in the second half. The taxonomic composition includes 83 taxa. At the beginning of this interval, the abundance of *L. sakaii* F.1 is high (up to 69.9%), followed by its sharp decrease from the middle of the interval. Frequent small peaks of the abundance of the species *Sethoconus tabulatus* (Ehrenberg, 1873) are also noteworthy (up to 1.0%). Several stratigraphically important events are recorded in this interval: LCO and LO of *L. sakaii* F.1 and FO of *Dictyophimus* sp. (Fig. 3). Also, the taxa *L. sakaii* F.2, *Amphisphaera cronos* Haeckel, 1887, *Actinomma leptodermum* (Jørgensen, 1900), *Spongodiscus resurgens* Ehrenberg, 1854, *Cornutella annulata* (Bailey, 1856), *Cycladophora cornuta* (Bailey, 1856), *Clathrocycloma* sp., *Cladoscenium ancoratum* Haeckel, 1887, *Lophophaena witjazii* (Petrushevskaya, 1971) Van de Paverd, *Pseudodictyophimus gracilipes* (Bailey, 1856) *bicornis* (Ehrenberg, 1872), *Artostrobium botryocyrtium* (Haeckel, 1887), *C. spinosus*, *Plegmosphaera* sp., etc., occur for the last time in this interval. Presence of a specimen of the Early–Middle Miocene species *Lipmanella pilva* Vitukhin, 1993 in the assemblage is noteworthy.

In the cold MIS 2 interval (177–108 cm, 28–14.69 kyr), TRC decreases to 995–3435 skeletons/g; the taxonomic composition includes 60 taxa. The taxon *Dictyophimus* sp. develops throughout this interval; its appearance was recorded in the middle of MIS 3. The abundance of this taxon is low (0.5–1.2%); however, it is found in almost all intervals and disappears at the MIS 2–MIS 1 boundary. In addition, the LO of *D. rectum* is recorded in the middle of this inter-

val. Also, the taxa *Cenosphaera cristata* Haeckel, 1887, *Actinomma* sp., *Cromyechinus borealis* (Cleve, 1898), *Sethoconus* sp., *Lophophaena simplex* Funakawa, 1994, *Helotholus hisrticosa* Jørgensen, 1905, *Cyrtopera laguncula* Haeckel, 1887, and *Pseudocubus* sp. F.2 occur for the last time in this interval. In addition, the assemblage contains taxa recorded only in this interval: *Thecosphaera pseudojaponica* Nakaseko, 1972, *Actinomma turidae* Kruglikova et Bjorklund, 2009, *Carpocanarium* sp., and *Lophophaena* ex gr. *cylindrica* (Cleve, 1899). This interval contains one specimen of the species *L. sakaii* F.1 and one specimen of *A. setosa*, as well as fragments of the Early–Middle Miocene taxon *Pentactinosphaera* sp., which indicates processes of reworking.

At the beginning of warm MIS 1 (105–0 cm, about 14.7–0 kyr), TRC is low, from 882 to 1971 skeletons/g; from the interval of 72–73 cm, it begins to sharply increase and reaches 7903–9780 skeletons/g. The taxonomic composition includes 63 taxa. The abundance of *C. davisiana* F.1 generally ranges from 2.8 to 19.0%; however, a sharp short-term outburst in abundance to 32.7–49.9% is observed in the middle of MIS 1, followed by its sharp decrease to 1.0–1.7% at the end of MIS 1 (Fig. 3). The same outbursts in abundance at the beginning of MIS 1 are demonstrated by the species *S. glacialis* (up to 46.8%) and the *S. stellata/validispina* species group (up to 23.8%), followed by a gradual decrease in their content towards the end of MIS 1.

DISCUSSION

Analysis of the taxonomic composition of radiolarians in the sediments of core LV76-9-1 revealed a high taxonomic diversity (129 taxa), but a low TRC compared to the central part of the Sea of Okhotsk (the highest TRC was 36 380 skeletons/g during the warm MIS 5.5 period). During interglacial periods, this content reaches 118 000–143 900 skeletons/g in the southern region of the central part (core MR06-04PC-07-R, Yanchenko and Gorbarenko, 2015, Yanchenko, 2019) and 90000–150000 skeletons/g in the northern region of the central part (core MD01-2415, Matul et al., 2009) (Fig. 1). However, the trend towards a decrease in TRC in glacial periods and its increase in interglacial periods applies for the entire Sea of Okhotsk. The highest abundance is recorded for several radiolarian species that sharply respond to temperature changes in the environment: *C. davisiana* F.1, *C. borealis* F.1, *S. stellata/validispina*, *S. glacialis*, *L. sakaii* F.1, *S. venustum*, etc.) (Fig. 3). A.G. Matul divided these and some other species into "glacial" and "interglacial" groups (2009).

In core LV76-9-1, the "glacial" group is dominated by the following species:

Cycladophora davisiana F.1 increases in the abundance during cold MIS 5.4 and at the beginning of MIS 5.2. However, its abundance sharply increases to 49.9% during warm MIS 3 and MIS 1. This is consistent with the data from Matul (2009), who revealed that high concentrations of *C. davisiana* in OM were observed in most of the glacial MISs throughout 1.1 Ma, although the maxima of the species abundance are also observed in a number of interglacial optima. *C. davisiana* F.2 is occasionally recorded at the end of MIS 5.3 (up to 0.9%) and in the middle of MIS 4 (1.1%) (Fig. 3). The short occurrence interval of this morphoform will likely allow its use for biostratigraphy.

Cerathospyris borealis F.1 reaches a high abundance (up to 14.9%) in the middle of cold MIS 5.2; however, its maximum abundance (up to 18.4%) was recorded at the end of MIS 3 (Fig. 3), followed by its decrease up to the middle of MIS 1. *C. borealis* F.2 forms small abundance peaks (up to 1.5%), mainly during MIS 5.5 and MIS 5.4, and sporadically occur in the upper part of the core after a long break, starting from MIS 3.

The *S. stellata/validispina* group reaches 21–26%, mainly during cold MIS 5.4, MIS 5.2, MIS 4, and MIS 2, as well as at the beginning of warm MIS 1, followed by a gradual decrease in its abundance.

Spongotrochus glacialis and *S. venustum* were assigned by Matul (2009) to the "glacial" group. However, their abundance in the sediments of the core that we studied from the southeastern part of the Sea of Okhotsk increases during warm MIS 5.1, MIS 5.3, and MIS 3 and at the beginning of MIS 1 (Fig. 3). The abundance of the species *S. venustum* sharply increases (up to 49.1%) only at the beginning of cold MIS 2. The opposite picture is observed in the central part of the Sea of Okhotsk. These species demonstrate an almost identical distribution and are characterized by an increase in their abundance during cold MISs (Matul, 2009; Yanchenko, 2019). Most likely, *S. glacialis* and *S. venustum* are opportunists and adapt well to changing environmental conditions.

In addition to the dominant species, the core also contains several species that are low in abundance (up to 3%) but, in our opinion, stratigraphically very significant; these species can also be attributed to the "glacial" group:

Dumetum rectum forms several peaks of 1–3% during MIS 4. A significant abundance peak of this species during MIS 4 in the Sea of Okhotsk was recorded by Matul (2009). We established the LO of *D. rectum* about 28–29 kyr, i.e., at the MIS 2 and MIS 3 boundary.

The abundance of *Dictyophimus* sp. (Pl. 2, Fig. 3) is up to 1%; however, it occurs in a narrow range from the middle of MIS 3 to the end of MIS 2 (Fig. 3). The highest frequency of occurrence of this species is observed during the cold MIS 2 period, at the end of which this species disappears. Its FO is dated to about 50–51 kyr and LO is about 14–15 kyr, i.e., at the MIS 1 and MIS 2 boundary. The short interval of

occurrence of this species allows us to consider it as a biostratigraphic marker (Vasilenko et al., 2023).

Lychnocanoma sakaii F.1 demonstrates a significant increase in its concentration during MIS 4 and at the beginning of MIS 3. For this species, we determined the LCO about 40–45 kyr and LO about 30–31 kyr. The date of LCO for this species was not previously established in the Sea of Okhotsk. The wide interval of 5 kyr is determined by the fact that the common occurrence of the species is recorded until 45 kyr, inclusive; however, it was again recorded once after a slight break at mark 40 ka. Presumably, its occurrence in the absence interval is so low that we did not record it in our preparations. Therefore, we expanded its LCO. The dating of the LO of the species is close to those established earlier: 28 ka (Matul et al., 2002), 34 ka (Matul et al., 2009), and 31.6 ka (Matul, 2009); however, it significantly differs from datings 47–49 kyr (Okazaki et al., 2003), 47–48 kyr (Okazaki et al., 2005), and 56–57 kyr (Takahashi et al., 2000; Okazaki et al., 2003). This difference may be explained by inaccuracies in the age models. However, the fact that the datings by Okazaki et al. (2003, 2005) and Takahashi et al. (2000) are close to our LCO values suggests that these authors mistook the LCO of the species for its FO.

Higher up the core section, single fragmentary specimens of the species *L. sakaii* F.1 are recorded at the beginning of MIS 2 and at the end of MIS 1, which, apparently, are redeposited. The presence of redeposition processes during these periods is confirmed by the occurrence of Early–Middle Miocene radiolarian species. The maximum abundance level (Acme) of *L. sakaii* F.1 is recorded in the interval of about 53–70 kyr (maximum 71.3%, about 63–64 kyr). In the northern region of the central part of the Sea of Okhotsk, the Acme of *L. sakaii* F.1 was recorded in the range of 70–77 (mean 74.5) kyr (Matul, 2002; Matul, 2009); in the southern region of the central part of the Sea of Okhotsk, this level is 60–72 kyr (Yanchenko and Gorbarenko, 2015; Yanchenko, 2019). The sharp increase in the concentration of *L. sakaii* F.1 in the sediments is explained by a poor taxonomic composition in the preparations (eight to 21 taxa). At the same time, a large number of specimens is recorded for this species, while other taxa are single with rare exceptions.

Lychnocanoma sakaii F.2 is represented in the sediments by single specimens with a relative abundance of 1.3–1.4% at the boundary between MIS 3 and MIS 4. The LO of *L. sakaii* F.2 is dated to at about 49–50 kyr.

Among the species of the "interglacial" group, the highest concentrations are recorded for the following species:

Amphimelissa setosa demonstrates an increase in its concentration to 13–15% at the beginning of MIS 5.4, which has several distinct peaks, followed by a gradual decrease in its abundance. In the central part of the Sea of Okhotsk, the concentrations of this species reach 35.5% during MIS 5.4 (Yanchenko, 2019). The most intensive but gradual decrease in the abundance of this species is observed at MIS 5.2. At the beginning of MIS 5.1, we established its LCO about 82–85 kyr. This date is close to 80–120 kyr, which was established in the Bering Sea (Ikenoue et al., 2016). We failed to establish the LO of the species, since specimens rarely occurred higher up the section, up to the end of MIS 1.

Siphocampe arachnea demonstrates two stages of increasing abundance from the middle of MIS 5.2 to the beginning of MIS 5.1 and in the middle of MIS 3, which is consistent with the data for the central part of the Sea of Okhotsk (Matul, 2009; Yanchenko, 2019).

Sethoconus tabulatus is found in sediments in small quantities (up to 1%); however, it forms frequent peaks during warm MIS 5.5, MIS 5.3, and MIS 3 and in the first half of MIS 1, which is also close to the data for the central part of the Sea of Okhotsk (Matul, 2009; Yanchenko, 2019).

CONCLUSIONS

As a result of our study, we established the concentrations of radiolarian species in core LV76-9-1 over the past 122 kyr. Comparison with the core data from the central part of the Sea of Okhotsk showed a significant difference in the TRC (by almost an order of magnitude) and a difference in the concentration of stratigraphically important radiolarian species in the assemblages. These large differences in the TRC are presumably explained by active hydrodynamics in the southeastern part of the Sea of Okhotsk (in particular, by the influence of the West Kamchatka Current), which determined the dissolution and reworking of radiolarian skeletons.

We carried out a revision of the key radiolarian species *C. davisiana*, *L. sakaii*, and *C. borealis*, which are predominant in the Sea of Okhotsk. This study made it possible to divide them into morphoforms. In addition, age datings were established for several key species: LCO is dated to about 40–45 kyr, LO to about 30–31 kyr, and Acme to about 53–70 kyr for the species *L. sakaii* F.1; LCO is dated to about 82–85 kyr for the species *A. setosa*.

In addition to the previously established species, the developed age model and analysis of the taxonomic composition made it possible to classify species such as D. *rectum* (the disappearance of which was recorded at the boundary between MIS 2 and MIS 3 (LO ~ 28–29 kyr), and *Dictyophimus* sp. (with a short stratigraphic interval of existence from the middle of MIS 3 (LO ~ 50–51 kyr)) to the MIS 1 and MIS 2 boundary (LO ~ 14–15 kyr) as key radiolarian species.

Our research shows that biomarkers such as radiolarians are a relatively simple and less expensive tool for establishing the age of the Upper Pleistocene–Holocene sediments of the Sea of Okhotsk. The estab-

lished levels of FO, LO, and LCO of the species determine age limits without the use of difficult correlations. In addition, these levels indicate regional and global changes in the natural environment, which is important for paleoceanological reconstructions.

FUNDING

This study was supported by the Russian Science Foundation (grant no. 22-17-00118). The material for the study was obtained from budget of the Il'ichev Pacific Oceanological Institute, Far East Branch, Russian Academy of Sciences (state assignment, theme no. 124022100084-8). No additional grants were received to conduct or direct this specific study.

ETHICS APPROVAL AND CONSENT TO PARTICIPATE

This work does not contain any studies involving human or animal subjects.

CONFLICT OF INTEREST

The authors of this work declare that they have no conflicts of interest.

REFERENCES

Abelmann, A., Freeze-drying simplifies the preparation of microfossils, *Micropaleontology,* 1988, vol. 34, p. 361.

Abelmann, A., Brathauer, U., Gersonde, R., Sieger, R., and Zielinski, U., Radiolarian-based transfer function for the estimation of sea surface temperatures in the Southern Ocean (Atlantic sector), *Paleoceanography,* 1999, vol. 14, pp. 410–421.

Bosin, A., Gorbarenko, S., Shi, X., Liu, Y., and Zou, J., Regionalized primary paleoproduction variability in the Sea of Okhotsk during late Pleistocene and Holocene, *Asian J. Earth Sci.,* 2015, vol. 114, pp. 534–540.

Chen, Q., Cheng, X., Cai, Y., Luo, Q., Zhang, J., Tang, L., Hu, Y., Ren, J., Wang, P., Wang, Y., Zhang, Y., Xue, G., Zhou, J., Cheng, H., Edwards, R.L., and Hong, Z., Asian Summer Monsoon changes inferred from a stalagmite $\delta^{18}O$ record in central China during the Last Glacial period, *Front. Earth Sci.,* 2022, vol. 10, p. 863829.
https://doi.org/10.3389/feart.2022.863829

Channell, J.E.T., Xuan, C., and Hodell, D.A., Stacking paleointensity and oxygen isotope data for the last 1.5 Myr (PISO-1500), *Earth Planet. Sci. Lett.,* 2009, vol. 283, pp. 14–23.

Chen, S., Wang, Y., Cheng, H., Edwards, R.L., Wang, X., Kong, X., and Liu, D., Strong coupling of Asian Monsoon and Antarctic climates on suborbital timescales, *Sci. Rep.,* 2016, vol. 6, p. 32995.
https://doi.org/10.1038/srep32995

Gidrometeorologiya i gidrokhimiya morei. Okhotskoe more: Gidrokhimicheskie usloviya i okeanologicheskie osnovy formirovaniya biologicheskoi produktivnosti (Hydrometeorology and Hydrochemistry of the Seas. Sea of Okhotsk: Hydrochemical Conditions and Oceanological Basis for the Formation of Biological Productivity), St. Petersburg: Gidrometeoizdat, 1996, vol. 9, no. 2.

Gorbarenko, S.A., Stable isotope and lithologic evidence of late-glacial and Holocene oceanography of the northwestern pacific and its marginal seas, *Quat. Res.,* 1996, vol. 46, pp. 230–250.
https://doi.org/10.1006/qres.1996.0063

Gorbarenko, S.A., Khusid, T.A., Basov, I.A., Oba, T., Southon, J.R., and Koizumi, I., Glacial-Holocene environment of the southeast Okhotsk Sea: Evidence from geochemical and paleontological data, *Palaeogeogr., Palaeoclimatol., Palaeoecol.,* 2002a, vol. 177, pp. 237–263.

Gorbarenko, S.A., Nuernberg, D., Derkachev, A.N., Astakhov, A.S., Southon, J.R., and Kaiser, A., Magnetostratigraphy and tephrochronology of the Upper Quaternary sediments in the Okhotsk Sea: Implication of terrigenous, volcanogenic and biogenic matter supply, *Mar. Geol.,* 2002b, vol. 183, pp. 107–129.

Gorbarenko, S.A., Southon, J.R., Keigwin, L.D., Cherepanova, M.V., and Gvozdeva, I.G., 2004. Late Pleistocene–Holocene oceanographic variability in the Okhotsk Sea: geochemical, lithological and paleontological evidence, *Palaeogeogr., Palaeoclimatol., Palaeoecol.,* 2004, vol. 209, pp. 281–301.

Gorbarenko, S.A., Basov, I.A., Chekhovskaya, M.P., Southon, J., Khusid, T.A., and Artemova, A.V., Orbital and millennium scale environmental changes in the southern Bering Sea during the last glacial Holocene: geochemical and paleontological evidence, *Deep Sea Res., Part II,* 2005, vol. 52, pp. 2174–2185.

Gorbarenko, S.A., Goldberg, E.L., Kashgarian, M., et al., Millennium scale environment changes of the Okhotsk Sea during last 80 kyr and their phase relationship with global climate changes, *J. Oceanogr.,* 2007, vol. 63, no. 4, pp. 609–623.

Gorbarenko, S.A., Harada, N., Malakhov, M.I., et al., Responses of the Okhotsk Sea environment and sedimentology to global climate changes at the orbital and millennial scale during the last 350 kyr, *Deep Sea Res., Part II,* 2012, vols. 61–64, pp. 73–84.

Harada, N., Ahagon, N., Sakamoto, T., Uchida, M., Ikehara, M., and Shibata, Ya., Rapid fluctuation of alkenone temperature in the southwestern Okhotsk Sea during the past 120 kyr, *Global Planet. Change,* 2006, vol. 53, pp. 29–46.

Hendy, I.L. and Kennett, J.P., Tropical forcing of North Pacific intermediate water distribution during Late Quaternary rapid climate change? *Quat. Sci. Rev.,* 2003, vol. 22, pp. 673–689.

Ikenoue, T., Okazaki, Y., Takahashi, K., and Sakamoto, T., Bering Sea radiolarian biostratigraphy and paleoceanography at IODP Site U1341 during the last four million years, *Deep Sea Res., Part II,* 2016, vols. 125–126, pp. 38–55.

Itaki, T., Khim, B.K., and Ikehara, K., Last glacial–Holocene water structure in the southwestern Okhotsk Sea inferred from radiolarian assemblages, *Mar. Micropaleontol.,* 2008, vol. 67, nos. 3–4, pp. 191–215.

Kompleksnye issledovaniya ekosistemy Okhotskogo morya. Ekologiya morei Rossii (Integrated Studies of the Ecosystem of the Sea of Okhotsk. Ecology of Russian Seas), Sapozh-

nikov, V.V., Eds., Moscow: Izd. Vseross. Nauchno-Issled. Inst. Rybn. Khoz. Okeanogr., 1997.

Kruglikova, S.B., Radiolarians from the surface layer of sediments of the Sea of Okhotsk, in *Okeanologiya* (Oceanology), Moscow: Nauka, 1975, vol. 15, no. 1, pp. 116–122.

Kruglikova, S.B., *Radiolyarii—Polycystina iz donnykh otlozhenii Mirovogo okeana kak bioindikatory izmeneniya okruzhayushchei sredy* (Radiolarians—Polycystina from the bottom sediments of the World Ocean as bioindicators of environmental change), Moscow: GEOS, 2013.

Ling, H.Y., Polycystine radiolaria and silicoflagellates from surface sediments of the Sea of Okhotsk, *Bull. Geol. Surv. Taiwan,* 1974, vol. 24, pp. 1–11.

Martinson, D.G., Pisias, N.G., Hays, J.D., Imbrie, J., Moore, T.C. Jr., and Shackleton, N.J., Age dating and the orbital theory of the ice age: Development of a high-resolution 0 to 300,000-year chronostratigraphy, *Quat. Res.,* 1987, vol. 27, pp. 1–29.

Matul, A.G., *Chetvertichnaya biostratigrafiya i paleookeanologiya Okhotskogo morya i drugikh subarkticheskikh raionov* (Quaternary Biostratigraphy and Paleooceanology of the Sea of Okhotsk and Other Subarctic Areas), Moscow: GEOS, 2009.

Matul, A., Abelmann, A., Tiedemann, R., Kaiser, A., and Nürnberg, D., Late Quaternary polycystine radiolarian datum events in the Sea of Okhotsk, *Geo-Mar. Lett.,* 2002, vol. 22, pp. 25–32.
https://doi.org/10.1007/s00367-002-0093-y

Matul, A.G., Abelmann, A., Nürnberg, D., and Tiedemann, R., Stratigraphy and major paleoenvironmental changes in the Sea of Okhotsk during the last million years inferred from radiolarian data, *Oceanology,* 2009, vol. 49, pp. 93–100.

Nimmergut, A. and Abelmann, A., Spatial and seasonal changes of radiolarian standing stocks in the Sea of Okhotsk, *Deep Sea Res., Part I,* 2002, vol. 49, no. 3, pp. 463–493.

North Greenland Ice Core Project Members, High-resolution record of Northern Hemisphere climate extending into the last interglacial period, *Nature,* 2004, vol. 431, pp. 147–151.

Nürnberg, D., Dethleft, D., Tiedemann, R., Kaiser, A., and Gorbarenko, S.A., Okhotsk Sea ice coverage and Kamchatka glaciation over the last 350 ka—evidence from ice-rafted debris and planktonic $\delta^{18}O$, *Palaeogeogr., Palaeoclimatol., Palaeoecol.,* 2011, vol. 310, pp. 191–205.

Okazaki, Y., Takahashi, K., Yoshitani, H., et al., Radiolarians under the seasonally sea-ice covered conditions in the Okhotsk Sea: flux and their implications for paleoceanography, *Mar. Micropaleontol.,* 2003, vol. 49, pp. 195–230.

Okazaki, Y., Takahashi, K., Itaki, T, and Kawasaki, Y., Comparison of radiolarian vertical distributions in the Okhotsk Sea near the Kuril Islands and in the northwestern North Pacific off Hokkaido Island, *Mar. Micropaleontol.,* 2004, vol. 51, nos. 3–4, pp. 257–284.

Okazaki, Y., Takahashi, K., Katsuki, K., Ono, A., Hori, J., Sakamoto, T., Uchida, M., Shibata, Y., Ikehara, M., and Aoki, K., Late Quaternary paleoceanographic changes in the southwestern Okhotsk Sea: Evidence from geochemical, radiolarian, and diatom records, *Deep Sea Res., Part II,* 2005, vol. 52, nos. 16–18, pp. 2332–2350.

Okazaki, Y., Seki, O., Nakatsuka, T., Sakamoto, T., Ikehara, M., and Takahashi, K., Cycladophora davisiana (Radiolaria) in the Okhotsk Sea: a key for reconstructing glacial ocean conditions, *J. Oceanogr.,* 2006, vol. 62, no. 5, pp. 639–648.

Riethdorf, J.-R., Nürnberg, D., Max, L., Tiedemann, R., Gorbarenko, S.A., and Malakhov, M.I., Millennial-scale variability of marine productivity and terrigenous matter supply in the western Bering Sea over the past 180 kyr, *Climate of the Past,* 2013, vol. 9, pp. 1345–1373.

Sakamoto, T., Ikehara, M., Aoki, K., Iijima, K., Kimura, N., Nakatsuka, T., and Wakatsuchi, M., Ice-rafted debris (IRD)-based sea-ice expansion events during the past 100 ka in the Okhotsk Sea, *Deep Sea Res., Part II,* 2005, vol. 52, pp. 2275–2301.

Shuntov, V.P., *Biologiya dal'nevostochnykh morei Rossii* (Biology of the Far Eastern Seas of Russia), Vladivostok: Izd. Tikhookean. Nauchno-Issled. Rybokhoz. Tsentra (TINRO-Tsentr), 2001.

Spratt, R.M. and Lisiecki, L.E., A Late Pleistocene sea level stack, *Climate of the Past,* 2016, vol. 12, pp. 1079–1092.
https://doi.org/10.5194/cp-12-1079-2016

Tada, R., Irino, T., and Koizumi, I., Land-ocean linkages over orbital and millennial timescales recorded in Late Quaternary sediments of the Japan Sea, *Paleoceanography,* 1999, vol. 14, no. 2, pp. 236–247.

Takahashi, K., Fujitani, N., Yanada, M., and Maita, Y., Long-term biogenic particle fluxes in the Bering Sea and the central subarctic Pacific Ocean, 1990–1995, *Deep Sea Res., Part I,* 2000, vol. 47, no. 9, pp. 1723–1759.

Tsoy, I.B. and Shastina, V.V., Cenozoic assemblages of siliceous microplankton from the sediments of the Terpeniya Ridge (Sea of Okhotsk), *Tikhookean. Geol.,* 2000, vol. 19, no. 4, pp. 105–115.

Tsoy, I.B. and Shastina, V.V., *Kainozoiskii kremnistyi mikroplankton iz otlozhenii Okhotskogo morya i Kurilo-Kamchatskogo zheloba* (Cenozoic Siliceous Microplankton from the Sediments of the Sea of Okhotsk and Kuril–Kamchatka Trench), Vladivostok: Dalnauka, 2005.

Vasilenko, L.N., Vasilenko, Yu.P., and Gorbarenko, S.A., Biostratigraphy of bottom sediments in the southeastern part of the Sea of Okhotsk based on radiolarian analysis, *Mikropaleontologiya: fundamental'nye problemy i vklad v regional'noe geologicheskoe izuchenie nedr. Trudy XVIII Vserossiiskogo mikropaleontologicheskogo soveshchaniya (g. Sankt-Peterburg, 30 oktyabrya-3 noyabrya 2023 g.)* (Micropaleontology: Fundamental Problems and Contribution to the Regional Geological Study of the Subsoil. Proc. 18th All-Russ. Micropaleontol. Meet. (St.-Petersburg, October 30–November 3, 2023), Tkachenko, M.A., Alekseev, A.S., Vishnevskaya, V.S., Grundan, E.L., and Tolmacheva, T.Yu., Eds., St. Petersburg: Vseross. Nauchno-Issled. Geol. Inst., 2023, pp. 200–205. ISBN 978-5-93761-876-4.

Vasilenko, Yu.P., Gorbarenko, S.A., Bosin, A.A., Shi, X., Chen, M.-T., Zou, J., Liu, Y., Artemova, A.V., Yanchenko, E.A., and Savenko, M.P., Millennial mode of variability of sea ice conditions in the Okhotsk Sea during the last glaciation (MIS 4–MIS 2), *Quat. Int.,* 2017, vol. 459, pp. 187–200.
https://doi.org/10.1016/j.quaint.2017.09.039

Wolff, E.W., Chappellaz, J., Blunier, T., Rasmussen, S.O., and Svensson, A., Millennial-scale variability during the last glacial: The ice core record, *Quat. Sci. Rev.,* 2010, vol. 29, pp. 2828–2838.

Yamamoto, Y., Yamazaki, T., Kanamatsu, T., Ioka, N., and Mishima, T., Relative paleointensity stack during the last 250 kyr in the northwest Pacific, *J. Geophys. Res.,* 2007, vol. 112, p. B01104.
https://doi.org/10.1029/2006JB004477

Yanchenko, E.A., Response of radiolarians to global orbital and millennial changes in the climate and environment of the Sea of Okhotsk in the Late Pleistocene and Holocene, *Cand. Sci. (Geol.-Mineral.) Dissertation*, Vladivostok: Tikhookean. Inst. Dal'nevost. Otd. Ross. Akad. Nauk, 2019.

Yanchenko, E. and Gorbarenko, S., Radiolarian responses of the central Okhotsk Sea to the global orbital and millennial scale climate oscillations over last 90 kyr, *Asian J. Earth Sci.,* 2015, vol. 114, pp. 601–610.

Channell, J.E.T., Hodell, D.A., Crowhurst, S.J., Skinner, L.C., and Muscheler, R., Relative paleointensity (RPI) in the latest Pleistocene (10–45 ka) and implications for deglacial atmospheric radiocarbon, *Quat. Sci. Rev.,* 2018, vol. 191, pp. 57–72.
https://doi.org/10.1016/j.quascirev.2018.05.007

Translated by D. Zabolotny